Acta Cryst E CRYSTALLOGRAPHIC COMMUNICATIONS

ISSN 2056-9890

Structural characterization of 2-amino-6-hydroxybenzothiazole by single-crystal X-ray diffraction, Hirshfeld surface analysis and DFT calculations

Dilshoda Amanova,[a] Zubaydabegim Radjabova,[b]* Sardor Murodov,[b,c] Sevinch Erkinboyeva,[b] Odil Choriev,[d] Jamshid Ashurov[d] and Shahlo Daminova[b,c]

[a]Termez Branch of Tashkent State Medical University, 64 Islom Karimov Street, Termiz 132000, Uzbekistan, [b]National University of Uzbekistan named after Mirzo Ulugbek, University Street, 4, Tashkent 100174, Uzbekistan, [c]Uzbekistan-Japan Innovation Centre of Youth, University Street 2B, Tashkent 100095, Uzbekistan, and [d]Institute of Bioorganic Chemistry, Academy of Sciences of Uzbekistan, Mirzo Ulugbek Street 83, Tashkent 100125, Uzbekistan. *Correspondence e-mail: logica.08122003@gmail.com

Received 31 August 2026
Accepted 19 October 2026

Edited by N. Alvarez Failache, Universidad de la Repüblica, Uruguay

Keywords: crystal structure; 2-amino-6-hydroxybenzothiazole; Hirshfeld surface; void analysis; DFT calculations.

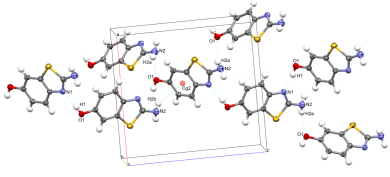
CCDC reference: 2596114

Supporting information: this article has supporting information at journals.iucr.org/e

2-Amino-6-hydroxybenzothiazole (or 2-amino-1,3-benzothiazol-6-ol), $C_7H_6N_2OS$, was synthesized by demethylation of the corresponding 2-amino-6-methoxybenzothiazole and crystallized from a DMF/acetone (2:3, *v*/*v*) solution. The molecule is essentially planar, with both the amino and hydroxy substituents lying close to the mean plane of the benzothiazole framework, reflecting an extended π-conjugated system. In the crystal, molecules are linked through O—H···N and N—H···O hydrogen bonds into chains propagating along the [001] direction, while weak N—H···π interactions further consolidate the packing. Hirshfeld surface analysis indicates that H···H, C···H/H···C, N···H/H···N, O···H/H···O and S···H/H···S contacts make the largest contributions to the intermolecular interactions. Density functional theory (DFT) calculations support the experimental molecular geometry and spectroscopic data and reveal a HOMO–LUMO energy gap of 5.09 eV, consistent with the good electronic stability of the molecule.

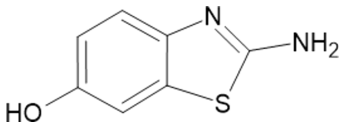
1. Chemical context

Benzothiazoles represent one of the most important classes of fused nitrogen- and sulfur-containing heterocyclic compounds owing to their remarkable structural diversity, ease of functionalization and broad spectrum of chemical, physical and biological properties. The benzothiazole scaffold has found widespread applications in medicinal chemistry, materials science, analytical chemistry and the development of functional organic compounds because of its chemical stability and the possibility of introducing a wide variety of substituents (Sharma *et al.*, 2013). In recent years, interest in this class of compounds has increased considerably, as evidenced by numerous comprehensive reviews focusing on the synthesis of benzothiazole derivatives and their pharmacological potential. Particular attention has been devoted to the development of new benzothiazole-based compounds with improved physicochemical properties, enhanced biological activity and greater structural diversity (Yadav *et al.*, 2023). The continuous development of benzothiazole chemistry has resulted in a wide range of synthetic methodologies. Classical approaches are mainly based on the cyclocondensation of 2-aminothiophenols, whereas more recent methods involve oxidative cyclization, one-pot synthetic strategies, transition-metal-catalysed reactions and environmentally benign protocols, allowing the preparation of structurally diverse benzothiazole derivatives in good to excellent yields (Gupta & Rawat, 2010).



OPEN ACCESS
Published under a CC BY 4.0 licence

Among benzothiazole derivatives, 2-aminobenzothiazoles occupy a unique position because the exocyclic amino group significantly expands the possibilities for further chemical functionalization. Consequently, these compounds are widely employed as synthetic intermediates for the preparation of Schiff bases, fused heterocyclic systems, azo compounds, functional materials and a variety of heterocyclic frameworks (Dadmal *et al.*, 2018). More recently, 2-aminobenzothiazoles have attracted considerable attention as versatile building blocks in multicomponent reactions, providing efficient access to structurally diverse nitrogen-containing heterocycles with high atom economy and operational simplicity. These developments have further expanded the synthetic utility of 2-aminobenzothiazole derivatives in modern organic chemistry (Javahershenas *et al.*, 2024). In addition to their synthetic importance, substituted 2-aminobenzothiazoles exhibit a broad spectrum of biological activities. Several newly synthesized derivatives have demonstrated significant anticancer activity against various tumour cell lines (Salih *et al.*, 2024), while others possess promising antifungal properties and are considered potential candidates for the development of new antimicrobial agents (Catalano *et al.*, 2013). The coordination ability of benzothiazole-based ligands has recently been demonstrated by the preparation of structurally diverse transition-metal complexes (Tojiboyeva *et al.*, 2025).
2-Amino-6-hydroxybenzothiazole is of particular interest because the simultaneous presence of a phenolic hydroxyl group, an exocyclic amino group and a benzothiazole ring provides multiple potential donor sites capable of participating in hydrogen bonding and metal coordination. Such structural features make this compound a promising N,O-donor ligand for the preparation of coordination compounds and functional molecular materials. Furthermore, derivatives of 2-aminobenzothiazole have also attracted attention in studies of microbial transformation and environmental degradation, highlighting the continuing scientific interest in this class of heterocyclic compounds (Bunescu *et al.*, 2008). Accordingly, the aim of the present work was to synthesize 2-amino-6-hydroxybenzothiazole (AGBT), obtain single crystals suitable for X-ray diffraction analysis, determine its molecular and crystal structure, investigate the intermolecular interactions by Hirshfeld surface analysis and crystal void analysis, and perform a computational study to gain further insight into its structural and electronic properties.



2. Structural commentary

The molecular structure of AGBT is shown in Fig. 1. The molecule is essentially planar, with the benzothiazole framework exhibiting a root-mean-square (r.m.s.) deviation from the least-squares plane of only 0.012 Å. Inclusion of the exocyclic amino group and the hydroxyl oxygen atom results

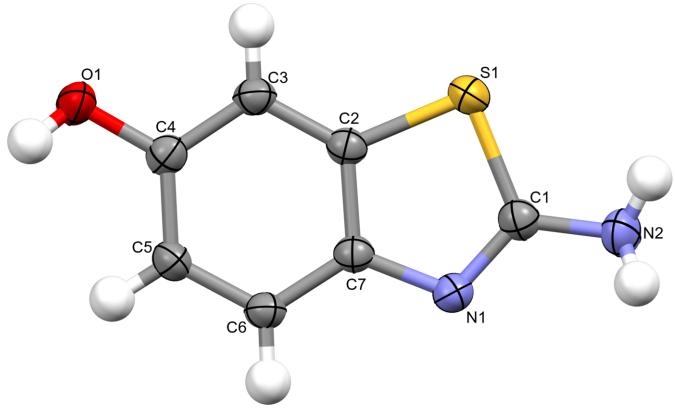


Figure 1
Molecular structure of AGBT with displacement ellipsoids drawn at the 50% probability level.

in only a slight increase of the r.m.s. deviation to 0.014 Å, indicating that both the benzothiazole skeleton and the substituent groups are nearly coplanar. The non-H atoms are nearly coplanar, as the geometry of the NH_2 group is pyramidal. The high degree of planarity reflects the presence of an extended π-conjugated system involving both the fused benzene and thiazole rings as well as the exocyclic functional groups. The negligible displacement of the hydroxyl and amino substituents from the least-squares plane of the benzothiazole framework suggests that these groups participate in the overall conjugated system, thereby promoting π-electron delocalization throughout the molecule. The bond distances within the benzothiazole ring are consistent with those expected for aromatic benzothiazole derivatives (Goubitz *et al.*, 2001). The C1═N1 bond length of 1.295 (3) Å confirms its pronounced double-bond character, whereas the C1—N2 bond length of 1.350 (4) Å is characteristic of an exocyclic amino substituent. The S1—C2 and S1—C1 bond lengths of 1.743 (2) and 1.761 (3) Å, respectively, are typical of aromatic benzothiazole systems possessing an extended π-conjugated framework. Likewise, the C4—O1 bond length of 1.367 (3) Å is characteristic of a phenolic C—O bond. The nearly ideal coplanarity of the molecule together with the observed bond-length distribution indicates substantial π-electron delocalization throughout the conjugated framework. This structural arrangement provides a rigid molecular geometry and preserves the coplanarity of the potential donor atoms, which is expected to be favourable for subsequent coordination with metal ions.

3. Supramolecular features

The crystal packing of AGBT is governed by a combination of classical O—H···N and N—H···O hydrogen bonds, which are further complemented by weak N—H···π interactions (Fig. 2 and Table 1). The strongest intermolecular interaction is an almost linear O1—H1···N1 hydrogen bond [O···N = 2.702 (3) Å, O—H···N = 173 (2)°]. These hydrogen bonds link adjacent molecules into infinite one-dimensional chains propagating along the [001] crystallographic direction. The

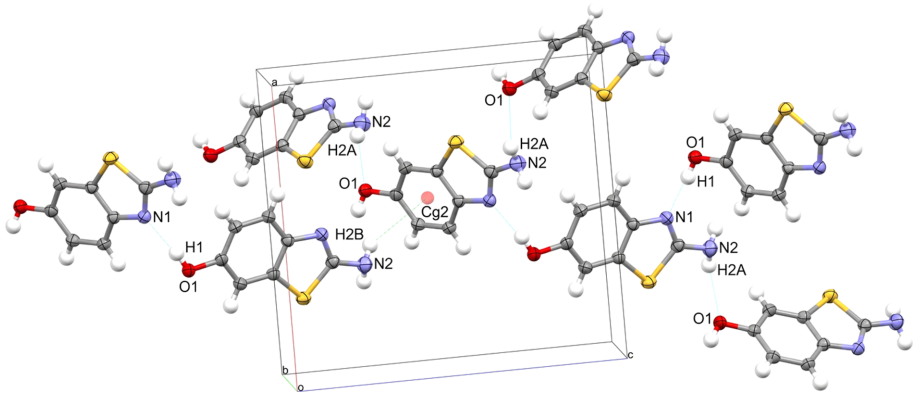


Figure 2
Crystal packing of AGBT showing the O—H···N and N—H···O hydrogen bonds (dashed lines) forming chains along the [001] direction.

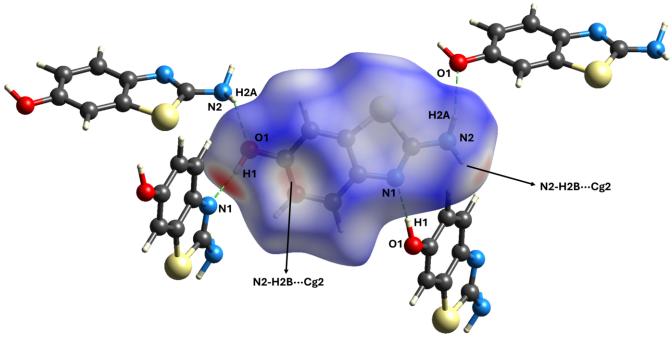


Figure 3
Hirshfeld surface of AGBT mapped over d_{norm}, highlighting the intermolecular O—H···N and N—H···O hydrogen-bonding interactions as red spots.

nearly linear geometry indicates the strong nature of this interaction, which represents the primary driving force governing the crystal packing. The resulting chains are further interconnected through N2—H2*A*···O1 hydrogen bonds [N···O = 2.920 (3) Å, N—H···O = 137.9 (14)°], thereby reinforcing the supramolecular assembly and contributing to the overall stability of the crystal structure. In addition to the classical hydrogen bonds, a weak N2—H2*B*···π interaction is observed between the amino group and the centroid (*Cg*2) of the C2–C7 benzene ring of a neighbouring molecule. The geometric parameters of this contact [H···*Cg* = 2.960 (13) Å, N···*Cg* = 3.705 (3) Å, N—H···*Cg* = 146.3 (12)°] fall within the typical range for N—H···π interactions and provide additional consolidation of the three-dimensional crystal packing.

Table 1
Hydrogen-bond geometry (Å, °).

*Cg*2 is the centroid of the C2–C7 ring.

D—H···*A*	*D*—H	H···*A*	*D*···*A*	*D*—H···*A*
O1—H1···N1^{i}	0.82 (2)	1.89 (2)	2.702 (3)	173 (2)
N2—H2*A*···O1^{ii}	0.86 (2)	2.23 (2)	2.920 (3)	138 (1)
N2—H2*B*···*Cg*2^{iii}	0.86 (1)	2.96 (1)	3.705 (3)	146 (1)

Symmetry codes: (i) $-x+1, -y, z-\frac{1}{2}$; (ii) $-x+\frac{3}{2}, y+1, z+\frac{1}{2}$; (iii) $-x+1, -y+1, z+\frac{1}{2}$.

4. Hirshfeld Surface and Void analysis

A Hirshfeld surface (HS) analysis was performed using *CrystalExplorer* 21.5 (Spackman *et al.*, 2021). The d_{norm}-mapped Hirshfeld surface (Fig. 3) exhibits intense red spots located around atoms O1, N1 and the hydrogen atoms of the hydroxyl and amino groups, indicating the shortest intermolecular contacts. These regions correspond to the strong O—H···N and N—H···O hydrogen bonds discussed in the supramolecular analysis. In addition, weak N—H···π interactions involving the amino group and the centroid (*Cg*2) of the benzene ring are also evident, further contributing to the cohesion of the crystal structure.

The corresponding two-dimensional fingerprint plots (Fig. 4) reveal that H···H contacts make the largest contribution to the Hirshfeld surface (25.6%), reflecting the close packing of neighbouring molecules. Significant contributions also arise from C···H/H···C (19.8%) and N···H/H···N (18.1%) contacts, while O···H/H···O interactions account for

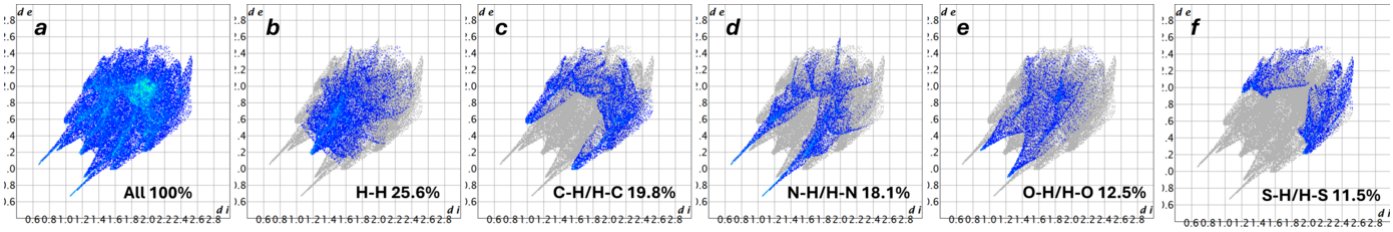


Figure 4
Two-dimensional fingerprint plots for AGBT showing the contributions of the principal intermolecular contacts: (*a*) overall fingerprint plot, (*b*) H···H, (*c*) C···H/H···C, (*d*) N···H/H···N, (*e*) O···H/H···O and (*f*) S···H/H···S contacts.

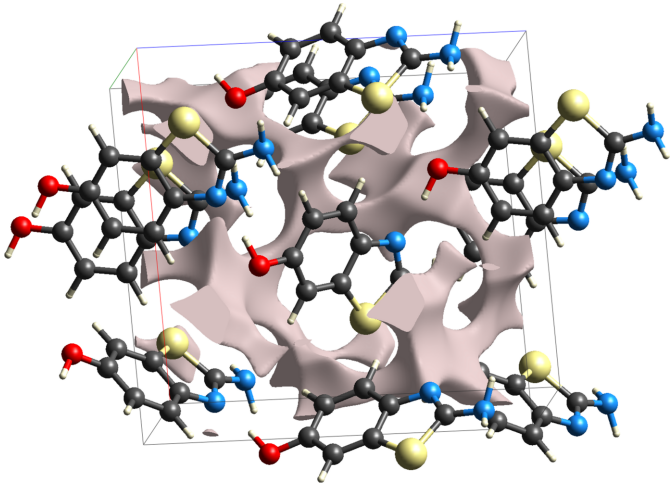


Figure 5
Crystal voids in AGBT calculated using a procrystal electron-density isovalue of 0.002 a.u.

12.5% of the total surface, confirming the important role of hydrogen bonding in the crystal packing. The contribution of S···H/H···S contacts amounts to 11.5%, whereas S···C/C···S (6.4%) and C···C (3.8%) interactions are considerably less significant. The very small contribution of C···C contacts indicates the absence of significant $\pi\cdots\pi$ stacking interactions in the crystal. The remaining contact types, including S···N/N···S (1.1%), S···O/O···S (0.6%), and O···C/C···O and N···C/C···N (0.3% each), make only minor contributions to the overall crystal packing.

To further evaluate the efficiency of crystal packing, a void analysis was performed (Fig. 5). The calculated void volume and void surface area are 68.47 Å^3 (9.4%) and 256.64 Å^2, respectively. The relatively small void volume indicates efficient packing of the molecules within the unit cell, which is consistent with the extensive network of intermolecular hydrogen bonds and additional N—H···π interactions. No large continuous cavities are present, indicating that the crystal structure is densely packed and efficiently consolidated by the cooperative intermolecular interactions.

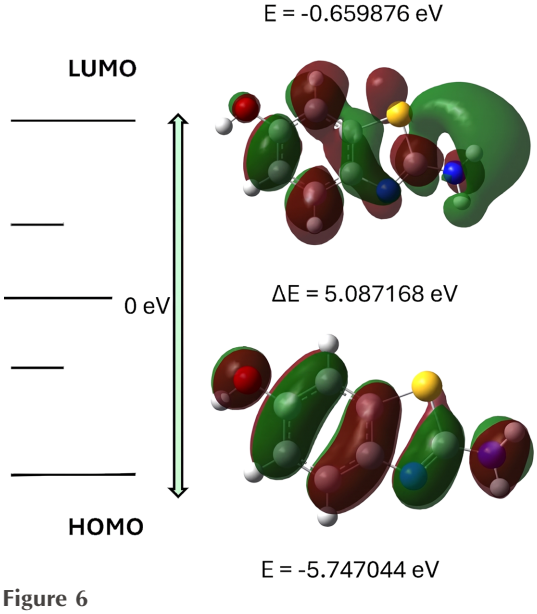


Figure 6
Frontier molecular orbitals of AGBT: HOMO and LUMO.

Table 2
Quantum-chemical properties.

Total energy (Hartree)	−853.438
E(HOMO) (eV)	−5.747
E(LUMO) (eV)	−0.660
Band gap, ΔE (eV)	5.087
Dipole moment (Debye)	1.292
Ionization potential, I (eV)	5.747
Electron affinity, A (eV)	0.660
Electronegativity, χ (eV)	3.204
Chemical potential, μ (eV)	−3.204
Global hardness, η (eV)	2.544
Global softness, S (eV-1)	0.197
Electrophilicity index, ω (eV)	2.02

5. Computational methods

Quantum-chemical calculations were performed using *Gaussian 16* (Frisch *et al.*, 2016). Geometry optimization and harmonic vibrational frequency calculations were carried out at the B3LYP/6-311++G(d,p) level of theory in the gas phase. Frequency calculations confirmed that the optimized geometry corresponds to a local minimum on the potential-energy surface, as no imaginary frequencies were found. Based on the optimized geometry, the frontier molecular orbitals (HOMO and LUMO) were analysed.

The calculated frontier molecular orbitals are shown in Fig. 6. The energies of the highest occupied and lowest unoccupied molecular orbitals are E(HOMO) = −5.747 eV and E(LUMO) = −0.660 eV, respectively, giving a HOMO–LUMO energy gap of 5.087 eV. The HOMO is mainly distributed over the π-conjugated benzothiazole framework with a contribution from the hydroxyl group, whereas the LUMO is localized predominantly on the benzothiazole fragment involving the heterocyclic carbon and nitrogen atoms. The calculated HOMO–LUMO energy gap characterizes the separation between the occupied and unoccupied frontier orbital energy levels at the selected level of theory. The calculated quantum-chemical descriptors derived from the frontier orbital energies are summarized in Table 2.

6. Database survey

A search of the Cambridge Structural Database (CSD, Version 5.47, update of June 2026; Groom *et al.*, 2016) revealed no crystal structures corresponding to 2-amino-6-hydroxy-1,3-benzothiazole, either as an isolated compound or as a ligand in a metal complex. A broader substructure search based on the 2-aminobenzothiazole framework yielded 1100 entries, whereas a more specific search incorporating an oxygen substituent at the 6-position returned 50 entries. Among the structurally related compounds, the closest

Table 3
Calculated thermodynamic, UV–Vis and IR properties.

Thermodynamic parameters		IR vibrational frequencies (cm^{-1})	
Zero-point correction (Hartree)	0.122520	ν(O—H) stretching	3844.7
Thermal correction to energy (Hartree)	0.131776	νas(NH_2) asymmetric stretching	3680.4
Thermal correction to enthalpy, ΔH (Hartree)	0.132720	νs(NH_2) symmetric stretching	3569.8
Thermal correction to Gibbs free energy, ΔG (Hartree)	0.088396	ν(C—H) aromatic stretching	3198.8–3153.4
TD–DFT electronic transitions		ν(C═N) benzothiazole ring	1665.3
S1 ($\pi\rightarrow\pi^*$)	277–280 nm	ν(C═C) aromatic ring	1606.4
S2 ($\pi\rightarrow\pi^*$)	254–258 nm	δ(NH_2) scissoring	1458.5
S3 ($\pi\rightarrow\pi^*$)	236–242 nm	ν(C—O) phenolic group	1313.3
S4 ($\pi\rightarrow\pi^*$)	216–220 nm	ν(C—S) + ring deformation	1054.5
S5 ($\pi\rightarrow\pi^*$)	188–205 nm		

analogue is 6-methoxy-1,3-benzothiazol-2-amine (CSD refcode XAYVIE; Saeed *et al.*, 2012), which crystallizes in the orthorhombic space group *Pbca*. In the crystal, N—H···N hydrogen bonds generate centrosymmetric $R_2^2(8)$ dimers, which are further connected into chains along the *b*-axis direction through N—H···O hydrogen bonds. Other closely related structures include 2-amino-6-methoxybenzothiazolium hydrogen sebacate dihydrate (EWOTUG; Sun *et al.*, 2011) and pentacarbonyl(6-methoxy-1,3-benzothiazol-2-amine)tungsten (DUXFEJ; Hu *et al.*, 2015), demonstrating the occurrence of this molecular framework in both protonated organic compounds and metal complexes.

Additional structurally related entries include 6-(trifluoromethoxy)-1,3-benzothiazol-2-amine (riluzole; LOHVEM01; Bharti *et al.*, 2023) and its cocrystal with succinic acid (NAQMOK; Mondal *et al.*, 2017). Although these structures contain the same 2-aminobenzothiazole core, they differ from the title compound in the nature of the substituent at the 6-position. In particular, the hydroxy group of the title compound can act as both a hydrogen-bond donor and an acceptor, potentially giving rise to different intermolecular interactions and crystal-packing arrangements compared with the corresponding methoxy- and trifluoromethoxy-substituted derivatives. Thus, the present structure provides a crystallographic characterization of 2-amino-6-hydroxy-1,3-benzothiazole not previously represented in the CSD version surveyed.

7. Synthesis and crystallization

2-Amino-6-hydroxybenzothiazole was synthesized from *p*-anisidine in two consecutive steps involving thiocyanative cyclization followed by O-demethylation (Fig. 7). 2-Amino-6-methoxybenzothiazole was prepared following a literature procedure (Khokhlova *et al.*, 2024). Potassium thiocyanate (29.9 g, 0.308 mol) was dissolved in glacial acetic acid (75 mL), and a solution of *p*-anisidine (10.6 g, 0.085 mol) in glacial acetic acid (40 mL) was added under stirring. The reaction mixture was cooled to 273–278 K, and a solution of bromine (6.5 mL) in glacial acetic acid (30 mL) was added dropwise while maintaining the reaction temperature below 263 K. After stirring for 1 h at 278 K, the mixture was allowed to warm to room temperature and stirred for an additional 18 h. The reaction mixture was poured onto crushed ice and neutralized with 25% aqueous ammonia to pH ≃ 8. The resulting precipitate was collected by filtration, washed thoroughly with water, dried under reduced pressure and recrystallized from ethanol to afford 2-amino-6-methoxybenzothiazole as pale-yellow crystals in 86% yield.

2-Amino-6-hydroxybenzothiazole was obtained by O-demethylation of the corresponding methoxy derivative following a literature procedure with minor modifications (Gross *et al.*, 2016). A solution of 2-amino-6-methoxybenzothiazole in anhydrous dichloromethane (30 mL g^{-1}) was cooled to 273 K under a nitrogen atmosphere, and a 1.0 *M*

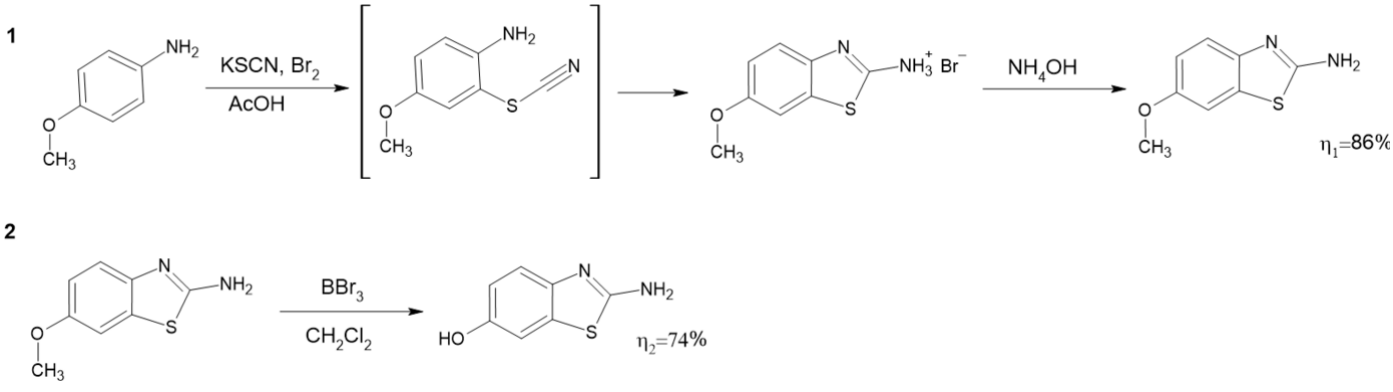


Figure 7
Synthesis of the title compound.

solution of boron tribromide in dichloromethane (1.5 equiv.) was added dropwise. After complete addition, the reaction mixture was allowed to warm to room temperature and stirred for 10–12 h. The reaction was carefully quenched with crushed ice and neutralized with saturated aqueous sodium hydrogen carbonate. The organic phase was separated, and the aqueous layer was extracted with dichloromethane. The combined organic extracts were dried over anhydrous sodium sulfate, filtered and concentrated under reduced pressure. Recrystallization from an ethanol/water mixture afforded 2-amino-6-hydroxybenzothiazole as pale-yellow crystals in 74% yield.

Single crystals suitable for X-ray diffraction analysis were obtained by slow evaporation of a solution of 2-amino-6-hydroxybenzothiazole in a mixed *N*,*N*-dimethylformamide/acetone (2:3, *v*/*v*) solvent system at room temperature.

^{1}H NMR (400 MHz, D_2O) δ 7.31 (*d*, *J* = 8.4 Hz, 1H, H-4), 7.18 (*d*, *J* = 2.2 Hz, 1H, H-7), 6.87 (*dd*, *J* = 8.4, 2.2 Hz, 1H, H-5). *^{1}H NMR (600 MHz, DMSO-d_6) δ 9.05 (*br s*, 1H, OH), 7.14 (*d*, *J* = 8.5 Hz, 1H, H-4), 7.02 (*br s*, 2H, NH_2), 6.96 (*d*, *J* = 2.3 Hz, 1H, H-7), 6.64 (*dd*, *J* = 8.5, 2.3 Hz, 1H, H-5). ^{13}C NMR (150 MHz, DMSO-d_6)* δ 163.5 (C-2), 152.0 (C-6), 144.1 (C-3a), 132.0 (C-7a), 118.2 (C-4), 113.8 (C-5), 106.1 (C-7).

The NMR spectra are fully consistent with the proposed structure of 2-amino-6-hydroxybenzothiazole (Bunescu *et al.*, 2008). The appearance of the characteristic OH and NH_2 resonances in the ^{1}H NMR spectrum recorded in DMSO-d_6, together with the absence of the methoxy signal observed for the precursor 2-amino-6-methoxybenzothiazole, confirms complete O-demethylation. The ^{13}C NMR spectrum exhibited seven carbon resonances corresponding to the seven chemically non-equivalent carbon atoms of the molecule. Calculated thermodynamic, UV–Vis and IR properties are summarized in Table 3.

8. Refinement

Crystal data, data collection and structure refinement details are summarized in Table 4. All non-hydrogen atoms were refined anisotropically. Hydrogen atoms bonded to carbon were positioned geometrically and refined using a riding model, with C—H = 0.93 Å and isotropic displacement parameters fixed at U_{iso}(H) = 1.2U_{eq}(C). The hydrogen atoms of the amino and hydroxyl groups were located from difference-Fourier maps and refined with restrained bond distances. Their isotropic displacement parameters were refined as U_{iso}(H) = 1.5U_{eq}(N,O) or 1.2U_{eq}(N) for the H atoms on N2.

Acknowledgements

The authors thank the Institute of Bioorganic Chemistry of the Academy of Sciences of Uzbekistan for providing access to the XtaLAB Synergy-S X-ray diffractometer. They also acknowledge the Uzbekistan-Japan Innovation Center of Youth for providing access to the analytical instrumentation and research facilities used in this work.

Table 4
Experimental details.

Crystal data	
Chemical formula	$C_7H_6N_2OS$
M_r	166.21
Crystal system, space group	Orthorhombic, $Pca2_1$
Temperature (K)	273
a, *b*, *c* (Å)	11.7093 (2), 4.9331 (1), 12.6026 (2)
V (Å^3)	727.97 (2)
Z	4
Radiation type	Cu *Kα*
μ (mm^{-1})	3.44
Crystal size (mm)	0.48 × 0.12 × 0.08
Data collection	
Diffractometer	XtaLAB Synergy, Single source at home/near, HyPix3000
Absorption correction	Multi-scan (*CrysAlis PRO*; Rigaku OD, 2023)
T_{min}, T_{max}	0.308, 1.000
No. of measured, independent and observed [$I \geq 2u(I)$] reflections	5514, 1256, 1212
R_{int}	0.034
(sin $\theta/\lambda)_{max}$ (Å^{-1})	0.615
Refinement	
$R[F^2 > 2\sigma(F^2)]$, $wR(F^2)$, *S*	0.034, 0.092, 1.05
No. of reflections	1256
No. of parameters	102
No. of restraints	1
H-atom treatment	H-atom parameters constrained
$\Delta\rho_{max}$, $\Delta\rho_{min}$ (e Å^{-3})	0.18, −0.21
Absolute structure	Hooft *et al.* (2010)
Absolute structure parameter	0.031 (14)

Computer programs: *CrysAlis PRO* (Rigaku OD, 2023), *SHELXT2018/2* (Sheldrick, 2015), *OLEX2.refine* (Bourhis *et al.*, 2015) and *OLEX2* (Dolomanov *et al.*, 2009).

References

Bharti, K., Dubey, G., Kumar, M., Jha, A., Manjit, Upadhyay, M., Mali, P. S., Kumar, A., Bharatam, P. V. & Mishra, B. (2023). *J. Drug. Deliv. Sci. Technol.* **90**, 105158.

Bourhis, L. J., Dolomanov, O. V., Gildea, R. J., Howard, J. A. K. & Puschmann, H. (2015). *Acta Cryst.* A**71**, 59–75.

Bunescu, A., Besse-Hoggan, P., Sancelme, M., Mailhot, G. & Delort, A. M. (2008). *Appl. Environ. Microbiol.* **74**, 2976–2984.

Catalano, A., Carocci, A., Defrenza, I., Muraglia, M., Carrieri, A., Van Bambeke, F., Rosato, A., Corbo, F. & Franchini, C. (2013). *Eur. J. Med. Chem.* **64**, 357–364.

Dadmal, T. L., Katre, S. D., Mandewale, M. C. & Kumbhare, R. M. (2018). *New J. Chem.* **42**, 776–797.

Dolomanov, O. V., Bourhis, L. J., Gildea, R. J., Howard, J. A. K. & Puschmann, H. (2009). *J. Appl. Cryst.* **42**, 339–341.

Frisch, M. J., Trucks, G. W., Schlegel, H. B., Scuseria, G. E., Robb, M. A., Cheeseman, J. R., Scalmani, G., Barone, V., Mennucci, B., Petersson, G. A., Nakatsuji, H., Caricato, M., Li, X., Hratchian, H. P., Izmaylov, A. F., Bloino, J., Zheng, G., Sonnenberg, J. L., Hada, M., Ehara, M., Toyota, K., Fukuda, R., Hasegawa, J., Ishida, M., Nakajima, T., Honda, Y., Kitao, O., Nakai, H., Vreven, T., Montgomery, J. A., Peralta, J. E., Ogliaro, F., Bearpark, M., Heyd, J. J., Brothers, E., Kudin, K. N., Staroverov, V. N., Kobayashi, R., Normand, J., Raghavachari, K., Rendell, A., Burant, J. C., Iyengar, S. S., Tomasi, J., Cossi, M., Rega, N., Millam, J. M., Klene, M., Know, J. E., Cross, J. B., Bakken, V., Adamo, C., Jaramillo, J., Gomperts, R., Stratmann, R. E., Yazyev, O. A., Austin, J., Cammi, R., Pomelli, C., Ochterski, J. O., Martin, R. L., Morokuma, K., Zakrzweski, V. G., Voth, G. A., Salvador, P., Dannenberg, J. J., Dapprich, S., Daniels, A. D., Farkas, O., Foresman, J. B., Ortiz, J. V., Cioslowski, J. & Fox, D. J. (2016). *AUSSIAN16.* Revision C.01. Gaussian Inc., Wallingford, CT, USA.

Goubitz, K., Sonneveld, E. J. & Schenk, H. (2001). *Z. Kristallogr.* **216**, 176–181.
Groom, C. R., Bruno, I. J., Lightfoot, M. P. & Ward, S. C. (2016). *Acta Cryst.* B**72**, 171–179.
Gross, T. D., Achampeta, R. P. & Citineni, J. R. (2016). US Patent 9,284,332.
Gupta, A. & Rawat, S. (2010). *J. Curr. Pharm. Res.* **3**, 13–23.
Hooft, R. W. W., Straver, L. H. & Spek, A. L. (2010). *J. Appl. Cryst.* **43**, 665–668.
Hu, S., Cui, X., He, W., Chen, X., Gu, Z., Zhao, J., Zeng, G., Shi, Z., Zhu, L. & Nie, H. (2015). *Z. Anorg. Allg. Chem.* **641**, 2452–2459.
Javahershenas, R., Han, J., Kazemi, M. & Jervis, P. J. (2024). ChemistryOpen 13, e202400185.
Khokhlova, E. A., Basanova, E. I., Serova, O. A., Bormotov, N. I., Skarnovich, M. O., Shishkina, L. N. & Nikitina, P. A. (2024). *Usp. Khim. Khim. Tekhnol.* **38**, 53–56.
Mondal, P. K., Rao, V., Mittapalli, S. & Chopra, D. (2017). *Cryst. Growth Des.* **17**, 1938–1946.
Rigaku OD (2023). *CrysAlis PRO*. Rigaku Oxford Diffraction, Yarnton, England.
Saeed, A., Rafique, H. & Flörke, U. (2012). *Acta Cryst.* E**68**, o2240.
Salih, O. M., Al-Sha'er, M. A. & Basheer, H. A. (2024). *ACS Omega* **9**, 13928–13950.
Sharma, P. C., Sinhmar, A., Sharma, A., Rajak, H. & Pathak, D. P. (2013). *J. Enzyme Inhib. Med. Chem.* **28**, 240–266.
Sheldrick, G. M. (2015). *Acta Cryst.* A**71**, 3–8.
Spackman, P. R., Turner, M. J., McKinnon, J. J., Wolff, S. K., Grimwood, D. J., Jayatilaka, D. & Spackman, M. A. (2021). *J. Appl. Cryst.* **54**, 1006–1011.
Sun, D., Li, Y.-H., Hao, H.-J., Liu, F.-J., Wen, Y.-M., Huang, R.-B. & Zheng, L.-S. (2011). *Cryst. Growth Des.* **11**, 3323–3327.
Tojiboyeva, I., Murodov, S., Makhmudova, L., Ziyatov, D., Ashurov, J. & Daminova, S. (2025). *Acta Cryst.* E**81**, 948–953.
Yadav, K. P., Rahman, M. A., Nishad, S., Maurya, S. K., Anas, M. & Mujahid, M. (2023). *Intell. Pharm.* **1**, 122–132.

supporting information

Acta Cryst. (2026). E**82** [https://doi.org/10.1107/S2056989026010819]

Structural characterization of 2-amino-6-hydroxybenzothiazole by single-crystal X-ray diffraction, Hirshfeld surface analysis and DFT calculations

Dilshoda Amanova, Zubaydabegim Radjabova, Sardor Murodov, Sevinch Erkinboyeva, Odil Choriev, Jamshid Ashurov and Shahlo Daminova

Computing details

2-Amino-1,3-benzothiazol-6-ol

Crystal data

$C_7H_6N_2OS$
M_r = 166.21
Orthorhombic, $Pca2_1$
a = 11.7093 (2) Å
b = 4.9331 (1) Å
c = 12.6026 (2) Å
V = 727.97 (2) Å^3
Z = 4
$F(000)$ = 346.387
D_x = 1.516 Mg m^{-3}
Cu $K\alpha$ radiation, λ = 1.54184 Å
Cell parameters from 4047 reflections
θ = 3.4–70.8°
μ = 3.44 mm^{-1}
T = 273 K
Needle, clear grayish white
0.48 × 0.12 × 0.08 mm

Data collection

XtaLAB Synergy, Single source at home/near, HyPix3000 diffractometer
Radiation source: micro-focus sealed X-ray tube, PhotonJet (Cu) X-ray Source
Mirror monochromator
Detector resolution: 10.0000 pixels mm^{-1}
ω scans
Absorption correction: multi-scan (CrysAlisPro; Rigaku OD, 2023)
T_{min} = 0.308, T_{max} = 1.000
5514 measured reflections
1256 independent reflections
1212 reflections with $I \geq 2u(I)$
R_{int} = 0.034
θ_{max} = 71.6°, θ_{min} = 7.0°
h = −14→14
k = −6→6
l = −14→15

Refinement

Refinement on F^2
Least-squares matrix: full
$R[F^2 > 2\sigma(F^2)]$ = 0.034
$wR(F^2)$ = 0.092
S = 1.05
1256 reflections
102 parameters
1 restraint
11 constraints
Primary atom site location: dual
H-atom parameters constrained
$w = 1/[\sigma^2(F_o^2) + (0.0568P)^2 + 0.1173P]$ where $P = (F_o^2 + 2F_c^2)/3$
$(\Delta/\sigma)_{max}$ = 0.0004
$\Delta\rho_{max}$ = 0.18 e Å^{-3}
$\Delta\rho_{min}$ = −0.21 e Å^{-3}
Absolute structure: Hooft *et al.* (2010)
Absolute structure parameter: 0.031 (14)

Fractional atomic coordinates and isotropic or equivalent isotropic displacement parameters (Å²)

	x	*y*	*z*	U_{iso}*/U_{eq}
S1	0.72738 (5)	0.52444 (11)	0.56161 (6)	0.0492 (2)
O1	0.63820 (16)	−0.1238 (5)	0.25086 (15)	0.0580 (5)
N1	0.53748 (17)	0.3383 (4)	0.64007 (18)	0.0432 (5)
N2	0.6301 (2)	0.6574 (5)	0.7480 (2)	0.0572 (6)
C7	0.55325 (17)	0.2101 (4)	0.54248 (19)	0.0388 (5)
C2	0.65307 (18)	0.2843 (5)	0.48723 (19)	0.0395 (5)
C3	0.68022 (19)	0.1784 (5)	0.3895 (2)	0.0443 (5)
C1	0.6202 (2)	0.5055 (5)	0.6594 (2)	0.0439 (6)
C4	0.6078 (2)	−0.0166 (5)	0.3468 (2)	0.0428 (6)
C6	0.4821 (2)	0.0154 (5)	0.4985 (2)	0.0435 (6)
C5	0.5105 (2)	−0.0990 (6)	0.4011 (2)	0.0447 (6)
H3	0.74499 (19)	0.2354 (5)	0.3531 (2)	0.0532 (7)*
H5	0.4638 (2)	−0.2321 (6)	0.3719 (2)	0.0536 (7)*
H6	0.4160 (2)	−0.0381 (5)	0.5338 (2)	0.0521 (7)*
H2a	0.6759 (17)	0.790 (3)	0.7361 (6)	0.0687 (7)*
H2b	0.5645 (4)	0.719 (4)	0.7666 (12)	0.0687 (7)*
H1	0.5816 (7)	−0.187 (8)	0.2217 (15)	0.0870 (8)*

Atomic displacement parameters (Å²)

	U^{11}	U^{22}	U^{33}	U^{12}	U^{13}	U^{23}
S1	0.0408 (3)	0.0528 (3)	0.0539 (4)	−0.0099 (2)	0.0031 (3)	−0.0072 (4)
O1	0.0434 (9)	0.0869 (14)	0.0437 (11)	−0.0023 (10)	0.0004 (8)	−0.0182 (11)
N1	0.0416 (9)	0.0471 (11)	0.0407 (11)	−0.0010 (8)	0.0036 (8)	−0.0012 (8)
N2	0.0561 (13)	0.0549 (13)	0.0606 (15)	−0.0006 (10)	0.0025 (11)	−0.0188 (11)
C7	0.0363 (10)	0.0396 (10)	0.0403 (13)	0.0011 (9)	0.0003 (9)	0.0020 (9)
C2	0.0355 (10)	0.0408 (11)	0.0424 (14)	0.0014 (9)	−0.0012 (9)	0.0018 (9)
C3	0.0351 (11)	0.0544 (14)	0.0434 (13)	−0.0011 (10)	0.0037 (10)	0.0016 (11)
C1	0.0406 (12)	0.0438 (12)	0.0473 (15)	0.0028 (9)	−0.0026 (11)	−0.0013 (10)
C4	0.0368 (12)	0.0525 (14)	0.0391 (13)	0.0079 (10)	−0.0026 (11)	−0.0003 (10)
C6	0.0351 (12)	0.0523 (14)	0.0430 (16)	−0.0030 (9)	0.0037 (10)	−0.0003 (10)
C5	0.0378 (11)	0.0510 (13)	0.0451 (15)	−0.0061 (10)	−0.0029 (10)	−0.0027 (11)

Geometric parameters (Å, º)

S1—C2	1.743 (2)	C7—C2	1.409 (3)
S1—C1	1.761 (3)	C7—C6	1.387 (3)
O1—C4	1.367 (3)	C2—C3	1.375 (4)
O1—H1	0.8200	C3—C4	1.390 (4)
N1—C7	1.395 (3)	C3—H3	0.9300
N1—C1	1.295 (3)	C4—C5	1.390 (4)
N2—C1	1.350 (4)	C6—C5	1.392 (4)
N2—H2a	0.8600	C6—H6	0.9300
N2—H2b	0.8600	C5—H5	0.9300

C1—S1—C2	89.11 (11)	H3—C3—C4	121.03 (16)
H1—O1—C4	109.5	N1—C1—S1	115.8 (2)
C1—N1—C7	110.8 (2)	N2—C1—S1	119.2 (2)
H2a—N2—C1	109.4	N2—C1—N1	125.0 (3)
H2b—N2—C1	110.3	C3—C4—O1	116.8 (2)
H2b—N2—H2a	109.5	C5—C4—O1	122.4 (2)
C2—C7—N1	115.3 (2)	C5—C4—C3	120.8 (3)
C6—C7—N1	125.9 (2)	C5—C6—C7	119.3 (2)
C6—C7—C2	118.7 (2)	H6—C6—C7	120.35 (15)
C7—C2—S1	108.96 (18)	H6—C6—C5	120.35 (14)
C3—C2—S1	128.64 (18)	C6—C5—C4	120.8 (2)
C3—C2—C7	122.4 (2)	H5—C5—C4	119.61 (16)
C4—C3—C2	117.9 (2)	H5—C5—C6	119.61 (14)
H3—C3—C2	121.03 (14)		

S1—C2—C7—N1	−0.39 (17)	C7—C2—S1—C1	0.10 (17)
S1—C2—C7—C6	−178.59 (16)	C7—C2—C3—C4	−2.6 (3)
S1—C2—C3—C4	178.8 (2)	C7—C6—C5—C4	−1.2 (3)
S1—C1—N1—C7	−0.5 (2)	C2—C7—N1—C1	0.6 (2)
O1—C4—C3—C2	−178.4 (2)	C2—C7—C6—C5	−0.6 (3)
O1—C4—C5—C6	−179.8 (3)	C2—C3—C4—C5	0.7 (3)
N1—C7—C2—C3	−179.3 (2)	C3—C2—S1—C1	178.9 (2)
N1—C7—C6—C5	−178.6 (2)	C3—C2—C7—C6	2.5 (3)
N1—C1—S1—C2	0.2 (2)	C3—C4—C5—C6	1.2 (3)
N2—C1—S1—C2	179.0 (2)	C1—N1—C7—C6	178.6 (2)
N2—C1—N1—C7	−179.2 (3)		

Hydrogen-bond geometry (Å, º)

*Cg*2 is the centroid of the C2–C7 ring.

D—H···*A*	*D*—H	H···*A*	*D*···*A*	*D*—H···*A*
O1—H1···N1^{i}	0.82 (2)	1.89 (2)	2.702 (3)	173 (2)
N2—H2A···O1^{ii}	0.86 (2)	2.23 (2)	2.920 (3)	138 (1)
N2—H2B···Cg2^{iii}	0.86 (1)	2.96 (1)	3.705 (3)	146 (1)

Symmetry codes: (i) −*x*+1, −*y*, *z*−1/2; (ii) −*x*+3/2, *y*+1, *z*+1/2; (iii) −*x*+1, −*y*+1, *z*+1/2.